Research Article
doi.org/10.1002/cbic.202300862
Chemistry Europe
European Chemical Societies Publishing

A Facile Access to Green Fluorescent Albumin Derivatives

Mario Saletti,[a] Marco Paolino,[a] Jacopo Venditti,[a] Claudia Bonechi,[a] Germano Giuliani,[a] Stefania Lamponi,[a] Giusy Tassone,[a] Antonella Boccia,[b] Chiara Botta,[b] Lluís Blancafort,[c] Federica Poggialini,[a] Chiara Vagaggini,[a] and Andrea Cappelli*[a]

A Morita-Baylis-Hillman Adduct (MBHA) derivative bearing a triphenylamine moiety was found to react with human serum albumin (**HSA**) shifting its emission from the blue to the green-yellow thus leading to green fluorescent albumin (**GFA**) derivatives and enlarging the platform of probes for aggregation-induced fluorescent-based detection techniques. A possible interaction of MBHA derivative **7** with a lipophilic pocket within the **HSA** structure was suggested by docking studies. DLS experiments showed that the reaction with **HSA** induce a conformational change of the protein contributing to the aggregation process of **GFA** derivatives. The results of investigations on the biological properties suggested that **GFA** retained the ability of binding drug molecules such as warfarin and diazepam. Finally, cytotoxicity evaluation studies suggested that, although the MBHA derivative **7** at 0.1 μg/mL affected the percentage of cell viability in comparison to the negative control, it cannot be considered cytotoxic, whereas at all the other concentrations $\geq$ 0.5 μg/mL resulted cytotoxic at different extent.

Introduction

In the past decades, protein labeling has been widely used in research and industry for biosensing, diagnostic imaging, targeted drug delivery, and other applications.[1] For example, most of the recent works have focused attention on the functionalization of proteins or antibodies, which can be used as drugs against cancer or infections.[2] The developed strategies are usually based on the reactivity of side chain residues of lysine and cysteine containing amino or thiol groups, respectively.[1] In particular, *N*-hydroxysuccinimide (NHS) esters,[3] isocianate (or thioisocianate),[4] and aldehydes for reductive amination[5] represent the most relevant functional groups exploited in the attack of the amino residue of lysine, while maleimides,[6] and α-halocarbonyls[7] are the main electrophiles used for the functionalization of the nucleophilic group of cysteines.[8] In addition, novel synthetic procedures involving selective metal-catalysed or metal-directed reactions, have been optimized.[9] However, these methods require the modification of the native protein (by chemical reactions or via genetic expressions) before its functionalization, which may involve complex synthetic steps and the possibility of chemo-functional alterations of the protein structure. Therefore, great efforts have been made to develop strategies to functionalize proteins at precisely defined sites while preserving their native functions and studying their structure-function relationships.[10–13]

In recent years, particular attention has been dedicated to the design of probes capable of tagging proteins in complex environments.[14–16]

Fluorescence-based detection techniques represent important tools in the study of protein interactions and function,[17] and fluorescent dyes are certainly at the bases of these techniques. However, in recent years, fluorogenic labeling strategies have demonstrated some important advantages such as the higher signal-to-noise ratio due to the fluorescence activation after its reaction/attachment to the desired site.[18–20] Furthermore, the fluorogens showing aggregation induced emission (AIE) features (i.e. emission intensities higher in the solid state than in solution)[21] display higher sensitivity, accuracy, and photostability when compared to traditional fluorescence probes, which are emissive in solution but often undergoes to aggregation caused quenching (ACQ) processes at high concentration.[22,23]

Some Morita-Baylis-Hillman derivatives (i.e. **1**, Figure 1) have been recently developed in our laboratories to react with imidazole[24] or *n*-butylammine[25] leading to cinnamic derivatives (i.e. **2**). showing fluorogenic properties. Although, these cinnamic derivatives displayed very weak emission in solution, methoxy and dimethoxy derivatives showed AIE features. In particular, compound **2** featured a bright blue emission with photoluminescence quantum yields (PL QY) around two orders of magnitude higher in the solid state with respect to the

[a] *M. Saletti, M. Paolino, J. Venditti, C. Bonechi, G. Giuliani, S. Lamponi, G. Tassone, F. Poggialini, C. Vagaggini, A. Cappelli*
Dipartimento di Biotecnologie, Chimica e Farmacia (Dipartimento di Eccellenza 2018–2022), Università degli Studi di Siena, Via Aldo Moro 2, 53100 Siena, Italy
Tel: +39 0577 232416
E-mail: andrea.cappelli@unisi.it

[b] *A. Boccia, C. Botta*
Istituto di Scienze e Tecnologie Chimiche "G. Natta" - SCITEC (CNR), Via A. Corti 12, 20133 Milano, Italy

[c] *L. Blancafort*
Institute of Computational Chemistry and Catalysis and Department of Chemistry, University of Girona, C/M. A. Capmany 69, 17003 Girona, Spain

Supporting information for this article is available on the WWW under https://doi.org/10.1002/cbic.202300862

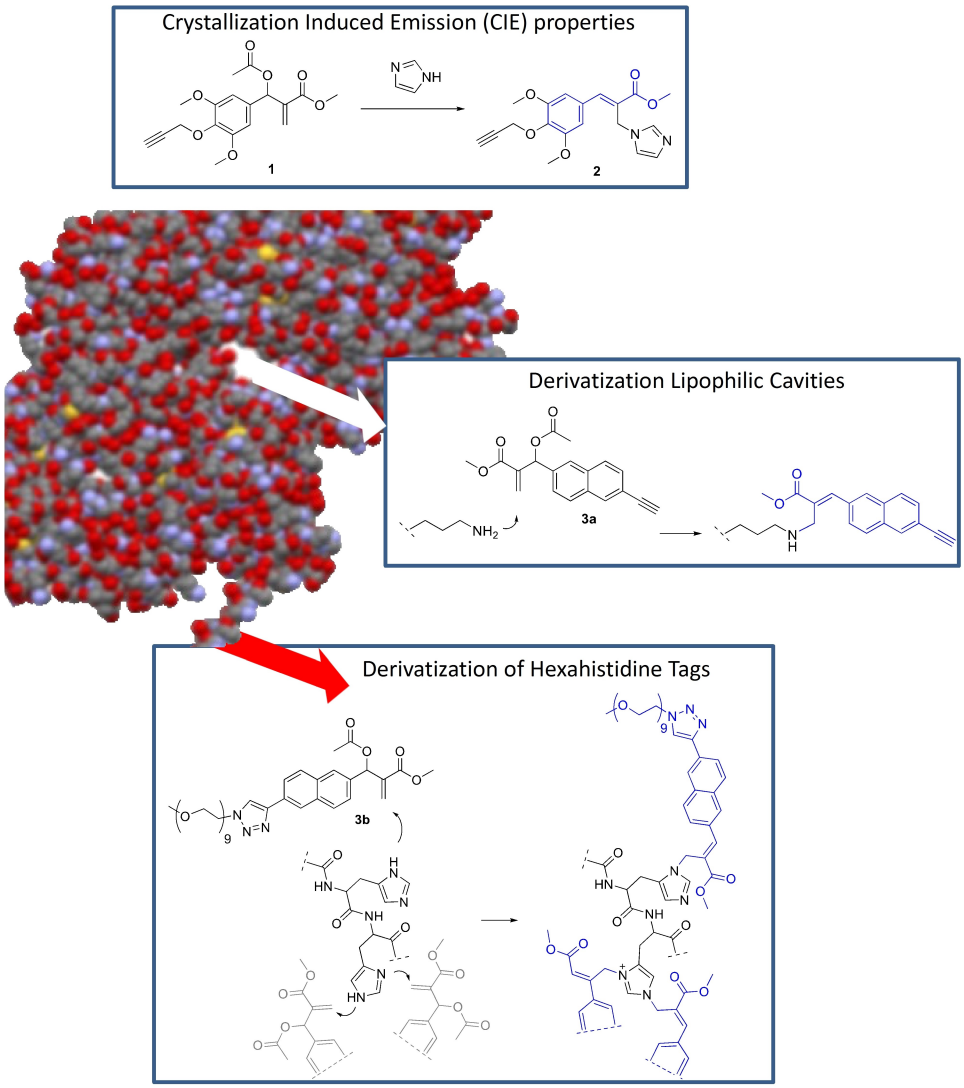

Figure 1. Structures of MBHA derivatives **1** leading to **2**, and MBHA derivatives **3 a,b** involved in site-specific protein derivatization.

corresponding values measured in solution, with the apparent presence of crystallization induced emission (CIE) phenomenon.[24]

In order to extend the π electron system, the phenyl group of these compounds (i.e. **1** and **2**) was then converted into the naphthalene nucleus (i.e. in compounds **3 a,b**), preparing fluorogenic molecules capable of generating monoadducts or diadducts compounds endowed with AIE properties.[26]

The reactivity of some naphthalene MBHA derivatives (i.e. **3 a,b**) was then studied in model proteins, and **3 a** was found to show a potential in the functionalization of lysine residues embedded in lipophilic pockets,[27] whereas **3 b** in the site-specific PEGylation of engineered proteins bearing poly-histidine tags.[28,29]

Very recently, we were successful in identifying cinnamic derivatives **4**, **5**, and **6** (Figure 2) as interesting fluorogenic

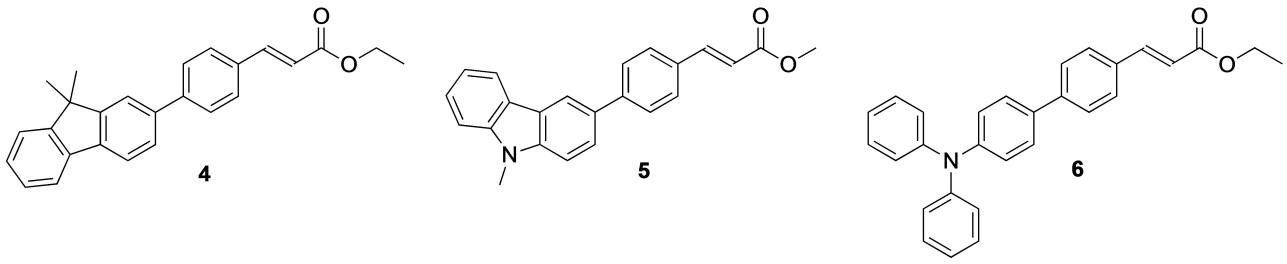

Figure 2. Structure of fluorescent cinnamic derivatives **4**, **5**, and **6**.

compounds showing photoluminescence quantum yield in the order of 57–80% and emission maxima in the range of 407–540 nm.[30]

The very promising photophysical features shown by triphenylamine cinnamic derivative **6** led to the development of the new fluorogenic probe **7**[31] potentially useful in the labeling of basic amino acid residues through an addition-elimination mechanism involving zwitterionic intermediates **8** and leading to cinnamic derivatives **9** (Figure 3).

Very intriguingly, the characterization of the photophysical and the photochemical features of MBHA derivative **7** provided us with very interesting results, confirming the promising photophysical features of the fluorophore contained in cinnamic derivatives **6, 11**, and **12**.[31] In particular, these studies demonstrated that the shift of the double bond from the acrylic structure of **7** and **10** to the cinnamic one of **6, 11**, and **12** produced a significant (130-150 nm) red shift in the emission of these compounds with photoluminescence quantum yield (PLQY) values around 58–80%.[31]

Thus, in the present work we investigated the reactivity features of MBHA derivative **7** in interacting with human serum albumin (**HSA**), which represents one of the most interesting proteins of human body. In fact, **HSA** is the most abundant protein in human plasma playing key roles in regulating the oncotic pressure and in carrying important endogenous (i.e. fatty acids, hormones, bilirubin etc.) and exogenous (i.e. drugs) substances. Moreover, **HSA** has been used in the development of drug delivery systems such as abraxane, a nanoparticle formulation of paclitaxel-loaded **HSA** used in the clinical treatment of metastatic breast cancer, small cell lung cancer, and advanced pancreatic cancer.[32,33]

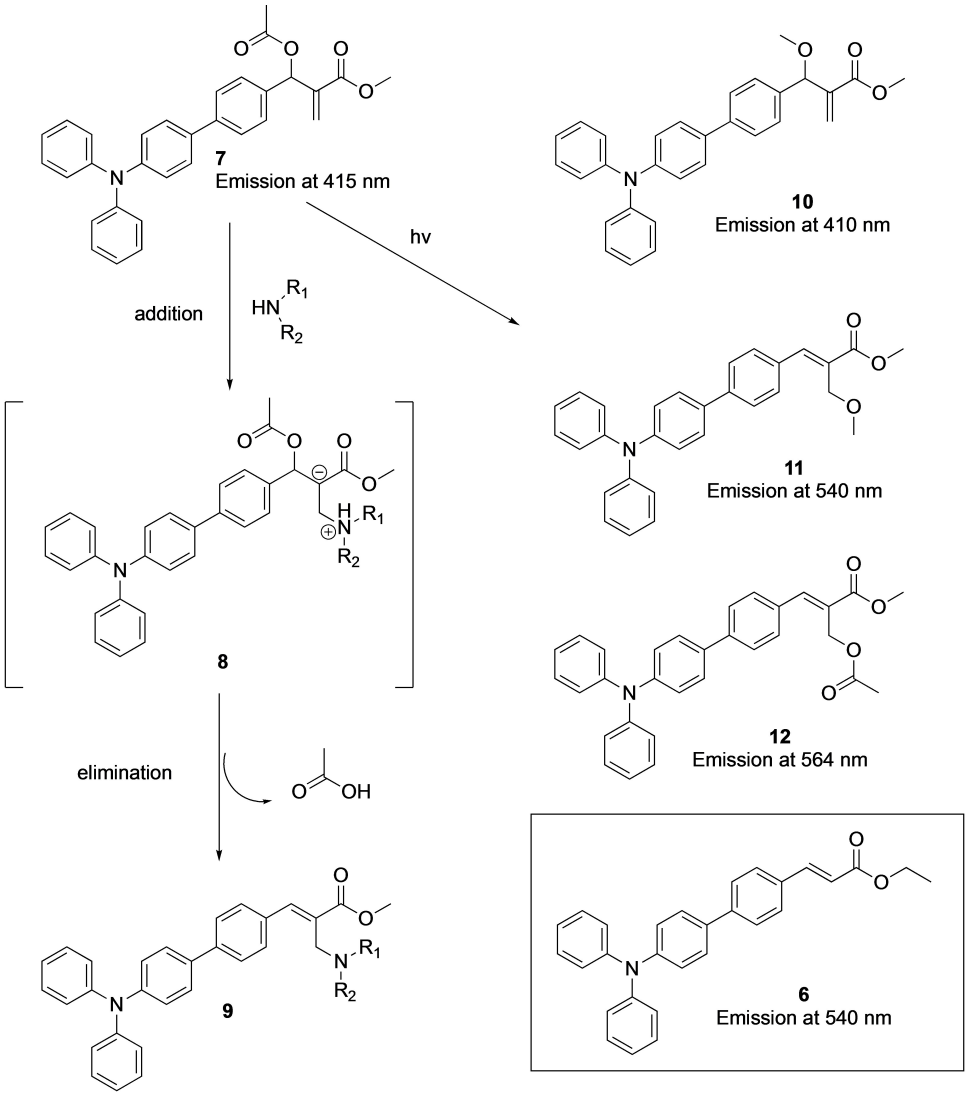

Figure 3. Structure of reactive MBHA derivative **7** leading to acrylic derivative **10** and cinnamic derivatives **9–12**.

Results and Discussion

Interaction of MBHA derivative 7 with HSA

The interaction of compound **7** with **HSA** was investigated by means of a range of different techniques such as Nuclear Magnetic Resonance (NMR) spectroscopy, absorption and emission spectroscopy, and computational docking simulations.

NMR. First, we started with a series of ^{1}H NMR experiments focused to detect the release of acetate during the elimination step following the initial addition step of the addition-elimination reaction involving a nucleophilic amino acid residue and MBHA derivative **7**. In particular, **HSA** (67 mg, 1.0 micromol) was dissolved in deuterium oxide (1.4 mL) containing phosphate buffered saline (PBS, 14 mg) at pH 7.4 into a 5 mm NMR tube and **7** (0.48 mg, 1.0 micromol) was added as a (50 mM) solution in deuterated dimethylsulfoxide (DMSO-d_6, 0.020 mL). The resulting reaction mixture was promptly analyzed by recording a ^{1}H NMR spectrum to obtain the information on the starting conditions (t = 0). The tube was then heated into an oil bath a 50 °C and ^{1}H NMR spectra were recorded at regular time intervals (i.e. 0, 1, 2, 4, 8, 24 h). The obtained spectra were elaborated all in the same manner and staked as shown in Figure 4.

The comparative analysis of the spectra showed that the shape of the **HSA** spectrum was stable in agreement with the reported stability of **HSA** solutions during prolonged heating at 60 °C.[34] Conversely, some visible differences can be easily attributed to the presence of MBHA derivative **7** and the small amount of DMSO added. In particular, while the apparent intensity of the signal at 2.66 ppm (assigned to DMSO added) was stable during the prolonged heating at 50 °C, the one of the signal at 1.88 ppm (assigned to acetate protons) increased progressively during the heating suggesting a progress of the addition-elimination reaction.

Very interestingly, all these events were paralleled by clear-cut changes in the fluorescence emission, which could be easily visualized by exposing the NMR tube-reactor to the UV lamp commonly used for TLC revelation at (365 nm) (Figure 5). In fact, the initial (t = 0) blue emission of MBHA derivative **7** (probably in aggregate form as suggested by its bright emission) progressively turned to the green-yellow during the prolonged heating at 50 °C, supporting the occurrence of the addition-elimination reaction leading to Green Fluorescent Albumin (**GFA**).

Absorption and emission spectroscopy. In Figure 6a the normalized absorption spectra of PBS and **HSA**-PBS in H_2O are compared with the absorption spectra of **7** in DMSO, **7** in DMSO-H_2O, and **7**-**HSA**-PBS in DMSO-H_2O. In Figure 6b the emission properties of **7** in DMSO and **7** in DMSO-H_2O solutions are shown. In Figure 6c and 6d the pictures of the solutions of **7**

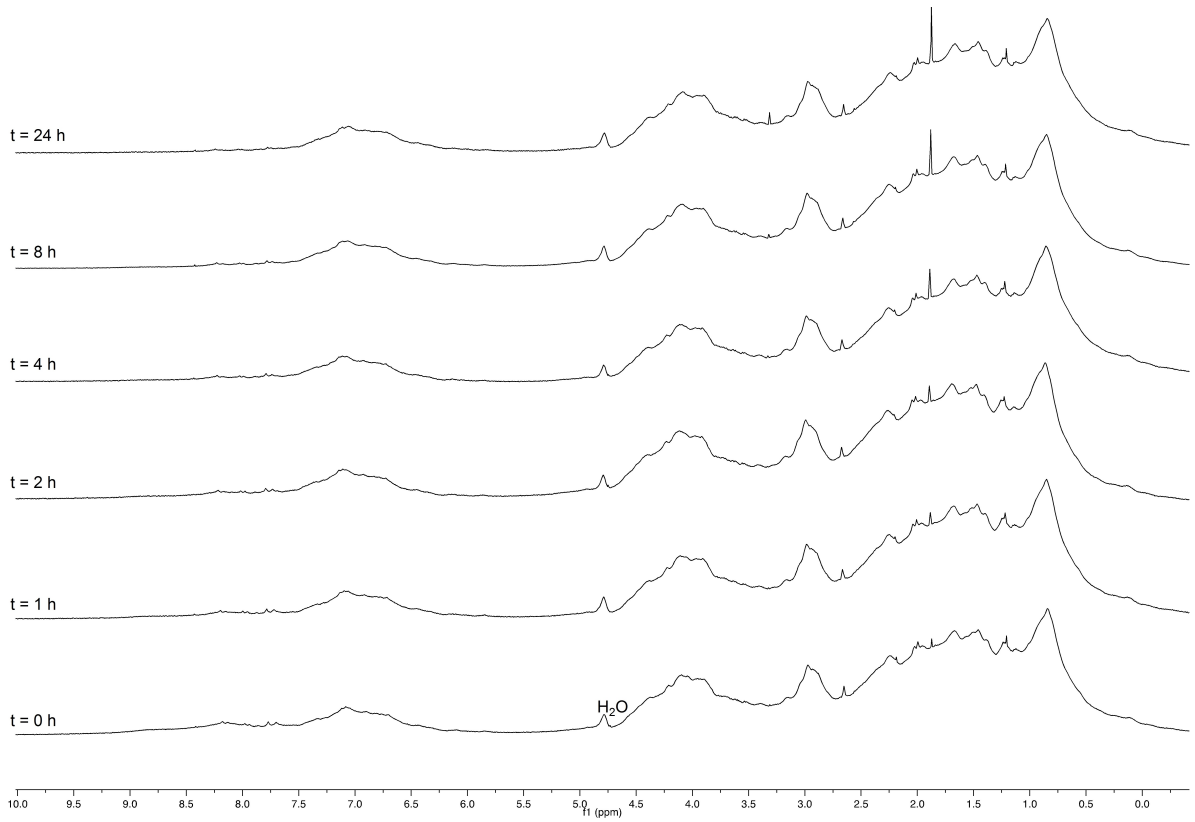

Figure 4. Comparison of the ^{1}H NMR (400 MHz) spectra of the reaction mixtures obtained with **HSA** (67 mg, 1.0 micromol) in D_2O (1.4 mL) containing solid PBS (Aldrich, 14 mg) at pH 7.4 and compound **7** (0.48 mg, 1.0 micromol), which was added as a (50 mM) solution in DMSO-d_6 (0.020 mL). The reaction mixtures contained into a 5 mm NMR tube were heated at 50 °C and ^{1}H NMR spectra were recorded at regular time intervals (0, 1, 2, 4, 8, and 24 h). The bottom trace was obtained with an **HSA** solution in D_2O.

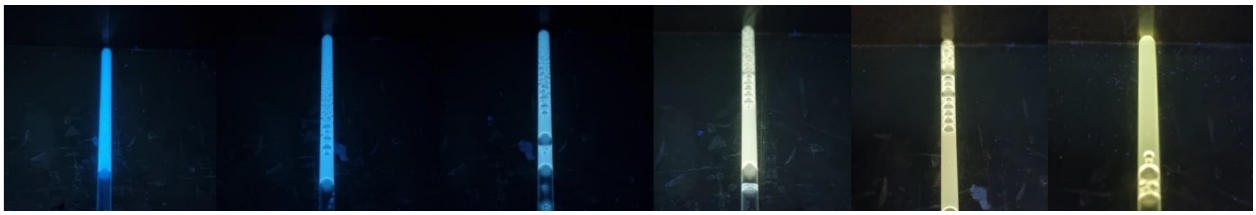

Figure 5. Comparison of the fluorescence emission of the reaction mixtures obtained with **HSA** (67 mg, 1.0 micromol) in D_2O (1.4 mL) containing PBS (Aldrich) at pH 7.4 and compound **7** (0.48 mg, 1.0 micromol), which was added as a (50 mM) solution in DMSO-d_6 (0.020 mL). The reaction mixtures contained into a 5 mm NMR tube were heated at 50 °C and were photographed at regular time intervals (0, 1, 2, 4, 8, and 24 h, from left to right in the sequence) under excitation at 365 nm.

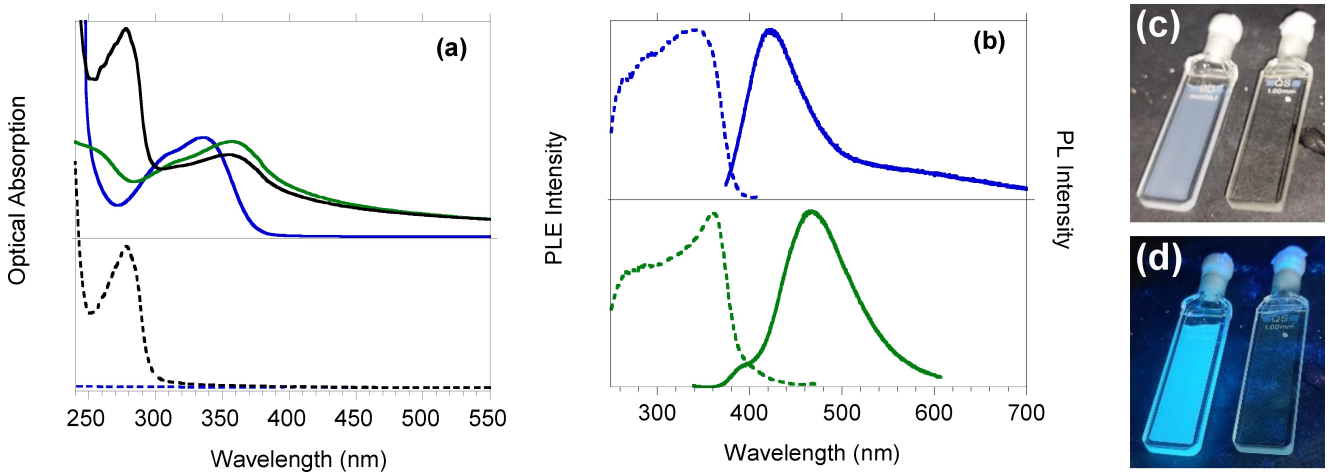

Figure 6. (a) Top: Absorption spectra of solutions of **7** in DMSO (blue solid line, [**7** (0.48 mg, 1.0 micromol) in DMSO (0.620 mL)]), **7** in DMSO-H_2O, (green solid line, [**7** (0.48 mg, 1.0 micromol) in DMSO (0.620 mL) and water (1.4 mL)]), **7**-**HSA**-PBS in DMSO-H_2O (black solid line, [**7** (0.48 mg, 1.0 micromol), **HSA** (67 mg, 1.0 micromol), PBS (14 mg) in DMSO (0.020 mL) and water (1.4 mL)]); Bottom: Absorption spectra of solutions of PBS in H_2O (blue dashed line, [PBS (14 mg) in water (1.4 mL)]), **HSA**-PBS in H_2O, (black dashed line, [**HSA** (67 mg, 1.0 micromol) and PBS (14 mg) in water (1.4 mL)]); (b) Top: PL and PLE spectrum of **7** in DMSO ([**7** (0.48 mg, 1.0 micromol) in DMSO (0.620 mL)]); Bottom: PL and PLE spectrum of **7** in DMSO-H_2O mixture [0.10 mL of [**7** (0.48 mg, 1.0 micromol) in DMSO (0.620 mL) and water (1.4 mL)] diluted in water (0.500 mL)]; $\lambda_{exc} = 330$ nm; $\lambda_{em} = 423$ nm (top); $\lambda_{em} = 480$ nm (bottom). (c,d) Photo of **7** in DMSO (right) [**7** (0.48 mg, 1.0 micromol) in DMSO (0.620 mL)] and DMSO-H_2O mixture (left) [**7** (0.48 mg, 1.0 micromol) in DMSO (0.620 mL) and water (1.4 mL)] in ambient light (c) and under UV lamp exposure (d).

in DMSO and **7** in DMSO-H_2O are shown both under ambient light and by UV lamp exposure.

The absorption spectrum of **7** red-shifted (from 336 nm to 356 nm) by adding water to the DMSO solution (see Figure 6a). This red-shift was a consequence of the formation of aggregates in the solution when the non-solvent (water) was added to the good solvent (DMSO). The formation of microaggregates was also responsible of light diffusion, giving the observed upshift of the absorption spectrum baseline (Figure 6a) and the opalescent aspect of the solution (Figure 6c). The red-shift observed in the absorption spectrum was very probably associated to the variation of the molecular conformation and/or to inter-molecular interactions occurring upon microaggregation. In fact, molecular planarization induces a red-shift in the absorption spectra and intermolecular interactions rigidify the molecular structure. The emission properties of rigidified molecules are enhanced thanks to the deactivation of intramolecular motions that in solution reduces radiative emission. This behavior is typical of AIE molecules with restricted intramolecular motions (RIM) properties in the solid state.[35,36]

Compound **7** displayed a very weak deep-blue emission (420 nm) when molecularly dissolved in a good solvent (DMSO) while its emission was strongly enhanced in intensity and shifted to 478 nm by adding water (bad solvent), as shown in Figure 6b. A similar behaviour was observed when a DMSO solution of **7** was added to the water solution of **HSA** (1.0 micromol) containing PBS (leading to **7**-**HSA**). The absorption spectrum of **7**-**HSA** (see Figure 6a) well corresponded to the absorptions of the different components (i.e. **HSA** shows a sharp peak at 277 nm while PBS did not absorb in the UV-Vis range). When excited at 360 nm, its PL spectrum was identical to that of **7** dissolved in a DMSO-water mixture while, upon exciting **HSA** at 277 nm, the emission of **HSA** was also observed at 332 nm (Figure ESI-1 and ESI-2).

The reaction of compound **7** with **HSA** was then monitored with a photoluminescence analysis of **7**-**HSA** solution during the heating process, in comparison with a reference solution of **7** in DMSO-H_2O subjected to the same heating treatment.

As shown in Figure 7, by heating the **7**-**HSA** solution, its PL spectrum showed a progressive red-shift from 480 nm to 525 nm and the solution became transparent (Figure 8a and

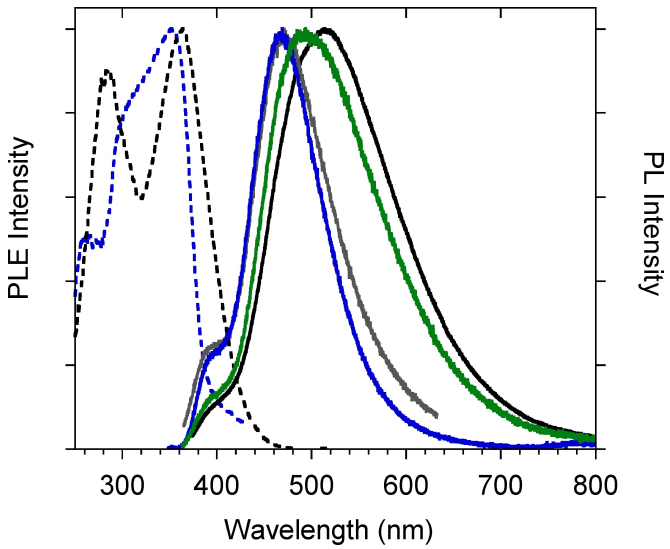

Figure 7. Normalized PL (solid lines, $\lambda_{exc} = 330$ nm) spectra of **7**-**HSA** solution during the heating treatment at 50 °C at different times (blue, pristine solution; grey, 2 h; green, 4 h; black, 8 h). Normalized PLE spectra (dashed lines) of the pristine solution (blue, $\lambda_{em} = 480$ nm) and after 8 h treatment at 50 °C (black, $\lambda_{em} = 525$ nm, [**7** (0.48 mg, 1.0 micromol), **HSA** (67 mg, 1.0 micromol), PBS (14 mg) in DMSO (0.020 mL) and water (1.4 mL)]).

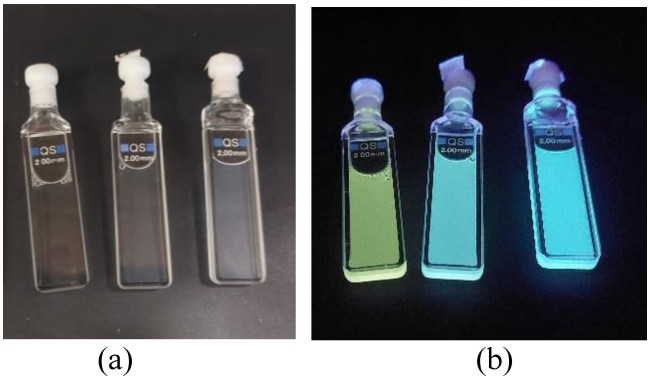

Figure 8. Photo of **7**-**HSA** solution heated at 50 °C for 8 h (left), pristine **7**-**HSA** solution (middle) and **7** DMSO-H_2O reference solution (right) heated at 50 °C for 8 h, in ambient light (a) and under UV irradiation (b). left and center: [**7** (0.48 mg, 1.0 micromol), **HSA** (67 mg, 1.0 micromol), PBS (14 mg) in DMSO (0.020 mL) and water (1.4 mL)]; right: [**7** (0.48 mg, 1.0 micromol) in DMSO (0.620 mL) and water (1.4 mL)].

Figure ESI-4) while no changes were observed for the reference solution (see Figure 7 and 8). This observation indicated that the thermal treatment of **7**-**HSA** modified the extent of micro-aggregation in solution, while no effects were observed for the reference solution of **7**. More interestingly, in Figure 7 a clear variation is observed after the thermal treatment in the PL excitation profiles (PLE) of **7**-**HSA** solution, showing a sharp peak at 280 nm that well corresponds to the absorption of **HSA** (see Figure 6a). This observation demonstrates that, in the **7**-**HSA** solution, **HSA** is able to transfer energy to **7** only after thermal treatment, indicating that the thermal treatment activates energy transfer by reducing the average distance between the two chromophores. By further dilution of the solution, energy transfer was observed to be independent on solution concentration. This fact, together with the red-shift of the emission, well supports the reaction between **HSA** and **7** leading to green fluorescent albumin (**GFA**). On the other hand, the persistence of **HSA** emission at 330 nm after the thermal treatment (see Figure ESI-2), showed the presence of **HSA** macromolecules non-coupled to **7**.

Docking simulations. Owing to the complexity of the **HSA** structure, the reactivity of MBHA derivative **7** could be rationalized by assuming initial non-covalent interactions with eventual binding sites on the **HSA** surface (or possibly with the pockets known to transport fatty acids and drugs) followed by the occurrence of the addition-elimination reaction with histidine, lysine, or arginine residues leading to the formation of covalent conjugates and to liberation of acetate ions. Thus, the interaction of MBHA derivative **7** with **HSA** was studied in silico by computational docking simulations to evaluate the possible existence of preferential non-covalent interaction sites, which could accommodate **7** allowing the reaction with the suitable nucleophilic amino acid residues. Our first step in this direction was to evaluate the accessible conformations of the protein through Molecular Dynamics (MD) simulations. Following this preliminary approach, molecular docking of **7** was then performed and the results obtained are shown in Figure 9.

The best pose of **7** was locate in the middle of the three I–II-III domains of the protein itself,[37] as showed in Figure 9. Analyzing the conformation clusters obtained, a versatile fitting of the ligand in this pocket was observed. This can be related to the relatively large size of the **HSA** pocket that allows the binding of **7** in many different manners. Comparing our results with the crystal structure of **HSA** complexed with warfarin (see Figure ESI-5),[38] we immediately notice similar (but not perfectly overlapping) poses of the two ligands within site I (of domain II) of **HSA**, as defined by Sudlow.[39] In fact, this high affinity binding site appears to be very large and adaptable, capable of binding bulky molecules such as bilirubin or different molecules in independent ways.[40] Considering the potential energy of ligand-protein complex obtained, the results showed a grid score of −46.5 kcal/mol,[41] suggesting a good accommodation of **7** within **HSA** structure. In particular, the contribution of the van der Waals energy is considerably greater (−45.7 kcal/mol) when compared to the value of the electrostatic energy (−0.8 kcal/mol). Similar results were observed for binding simulations in hydrophobic environment, where the entropic contribution appears to dominate the biomolecular associations mechanism.[42]

More in detail, compound **7** seems to fit perfectly into the pocket, placing the acrylic part inside the pocket and keeping the aromatic portion near the surface. This hydrophobic part of the molecule seems to interact with other aromatic residues present at the edge of the pocket (see Figure ESI-6 of the Supporting Information). Furthermore, confirming the hydrophobic nature of the pocket, no migration of water molecules within the binding site was observed in our 70 ns of simulation. The hydrogen bond (1.97 Å) between Arginine 257 and the carbonyl of the acrylic group is also shown in Figure 9. It seems to be a stable interaction between ligand and **HSA** but other nucleophilic residues, such as Lysine 199 and Histidine 242, are

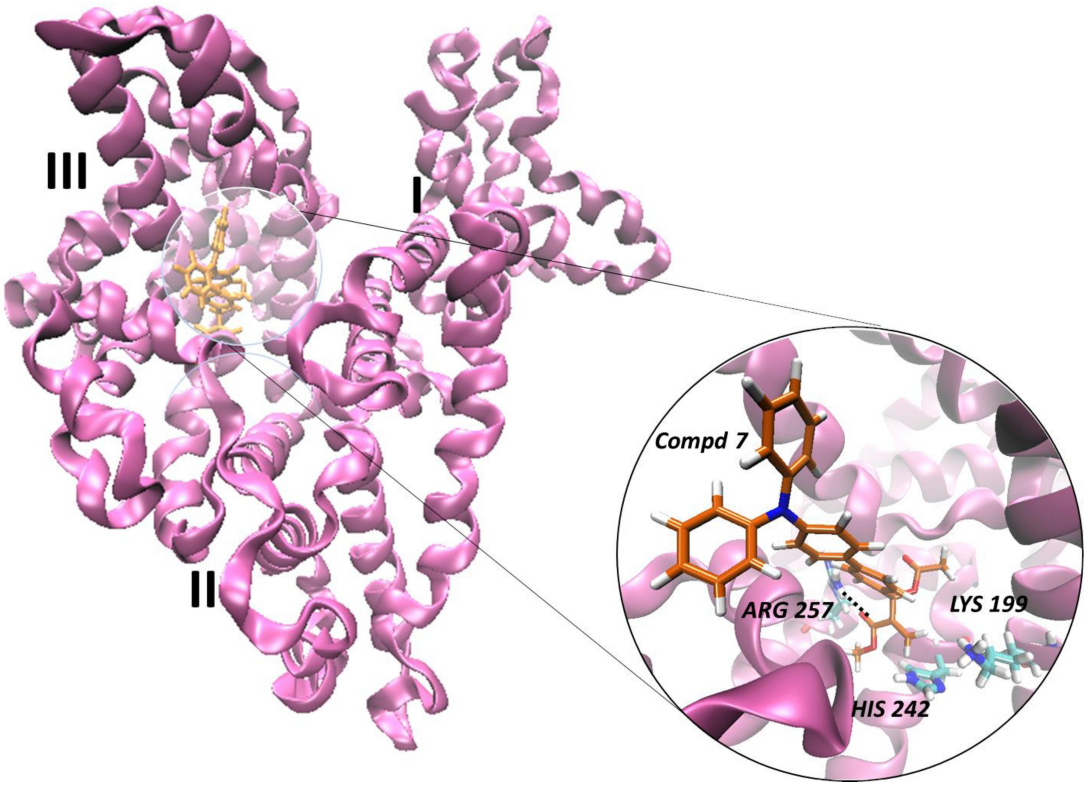

Figure 9. The most significant docking pose of MBHA derivative **7** within **HSA** structure.

also close to **7**. These residues do not yet appear to interact with the ligand but, proceeding with the MDs, they could determine alternative binding ways within the protein pocket. We refer particularly to the activated double bond of **7**, where the polarization of the electron cloud (the partial charges of **7** are reported in the Supporting Information), could promoting the addition-elimination reaction with the nearby residue Lys 199 (distance between C28 and N is 3.4 Å). It is noteworthy that Lys 199 was reported to be capable of reacting with aspirin by accepting the acetyl group of the drug molecule, suggesting a strong nucleophilic character.[43] This interesting feature could be determinant in the conjugation reaction following the initial recognition step. In other words, several important features appeared to suggest a potentially selective conjugation reaction of **7** with **HSA**: the affinity for the putative binding site, the strong nucleophilic character of Lys 199 and the correct orientation of the reacting groups.

Protein characterization

The product of the addition-elimination reaction (i.e. **GFA**) was characterized in comparison with the starting **HSA** by SDS page experiments and dynamic light scattering (DLS) measurements to ascertain the eventual existence of significant differences between **GFA** and starting **HSA** induced by the interaction with MBHA derivative **7**. Furthermore, the biological properties of **GFA** were evaluated in terms of the potential ability of binding drug molecules with respect to native **HSA**.

SDS page experiments. The high purity of the starting **HSA** protein sample and of the reaction product between **HSA** and MBHA derivative **7** after 24 h of incubation at 50 °C were confirmed through SDS-PAGE analysis (Figure 10). Both the

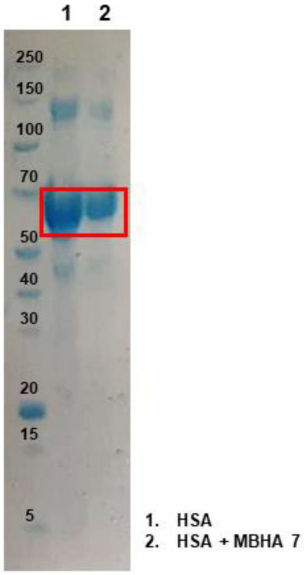

Figure 10. SDS-PAGE analysis (Bis-TRIS gel 4–12% NuPAGE, Thermo Fisher Scientific) of **HSA** (molecular weight 66472 Da) and the reaction product between **HSA** and MBHA derivative **7** after 24 h of incubation at 50 °C. The bands relating to both samples are highlighted in red. The marker used was the PageRuler Broad Range Unstained Protein Ladder (Thermo Fisher Scientific).

samples contained only one species as demonstrated by the presence of a single protein band after SDS-PAGE separation. This result confirmed the **HSA** stability in the mild reaction conditions. The small differences between the native protein and the derivatized sample **GFA** appeared to confirm the occurrence of derivatization reaction, but they could be not truly significant owing to the small value (i.e. 418 Da) of the chromophore with respect to the **HSA** molecular mass.

To verify the occurrence of derivatization, the resulting gel was exposed to the UV lamp (365 nm). However, no bands were discernible due to potential interference from the protein visualization dye (SimplyBlue™ SafeStain - Thermo Fisher). We assumed that the **GFA** emission (around 525 nm) could be quenched by the dye (i.e. comassie brilliant blue, absorption maximum at 595 nm) used in the SDS page experiments. To overcome this issue, electrophoretic analysis was performed again by loading the samples (**HSA** and the reaction product between **HSA** and MBHA derivative **7** after 24 hours of incubation at 50 °C) in duplicate. A section of the gel containing both samples was run following the previously described protocol, while the samples loaded as duplicates were loaded in the absence of the loading buffer (which contains the bromophenol blue as a dye, in its formulation). The first section of the gel was stained to allow the visualization of the samples, while the second section remained unstained and was subsequently exposed to UV lamp. The exclusion of dyes during sample preparation and visualization enabled the detection of an emissive band of green-yellow staining at the position (height) corresponding to the band of the derivatized protein, by comparison with the position of the band in the stained section of the gel.

Dynamic Light Scattering. DLS is a powerful technique that provides essential structural information about biological macromolecules in solution. In particular, DLS experiments allow the measurement of hydrodynamic diameter, polydispersity, and the presence of protein aggregates in solutions to be made. As reported in Table 1 and in Figure 11, the tendency

Table 1. Mean size, polydispersity index, and ζ-potential values of **GFA** compared to those of starting **HSA**.

Sample	Concentration	Size ± SD (nm)	Size ± SD (nm)	Size ± SD (nm)	PDI ± SD	ζ -potential ± SD (mv)
HSA	HSA (67 mg, 1.0 micromol) and PBS (14 mg) in water (1.4 mL)	8.91 ± 0.65	–	–	0.30 ± 0.13	-11.47 ± 0.64
GFA (Conc-Sol)	0.425 mL of [7 (0.48 mg, 1.0 micromol), HSA (67 mg, 1.0 micromol), PBS (14 mg) in DMSO (0.020 mL) and water (1.4 mL)] diluted in 1.0 mL of water	8.71 ± 0.75	50.0 ± 2.5	420.2 ± 6.3	0.40 ± 0.15	-19.05 ± 0.15
GFA (Dil-Sol)	0.275 mL [7 (0.48 mg, 1.0 micromol), HSA (67 mg, 1.0 micromol), PBS (14 mg) in DMSO (0.020 mL) and water (1.4 mL)] diluted in 1.0 mL of water	8.38 ± 0.87	91.8 ± 4.1	424.1 ± 7.1	0.46 ± 0.17	-18.37 ± 0.30

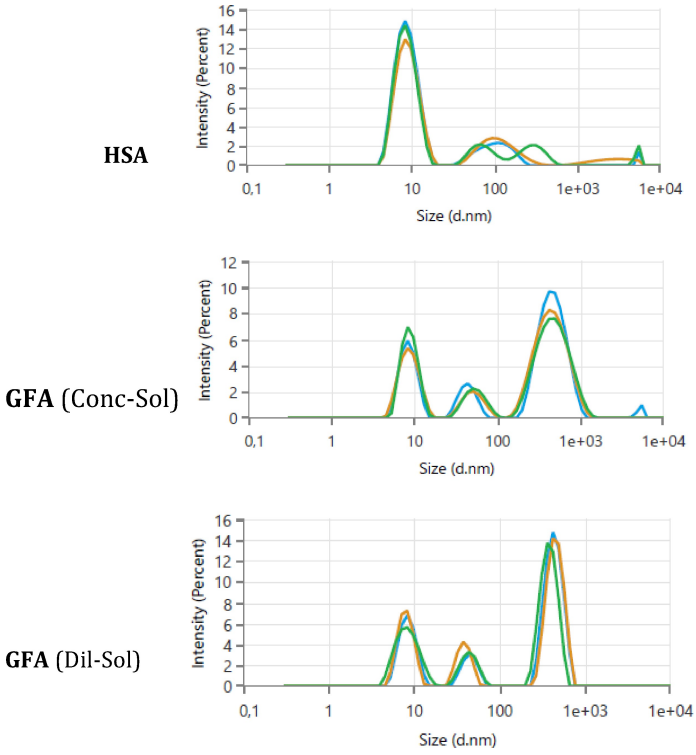

Figure 11. Size distribution profiles obtained by DLS experiments. The concentrations are reported in Table 1.

towards aggregation of **HSA** increases in **GFA** derivatives and this behavior was stable also to dilution.

In fact, DLS revealed in the **GFA** solution the presence of two populations of aggregates with dimension values of 50–92 nm and 420–424 nm, respectively. These results suggest that the reaction of **7** with **HSA** led to a conformational change of the protein.

The polydispersity index is a measure of the width of unimodal size distributions. The PDI of the **GFA** samples was generally low (~0.40), indicating good dispersion homogeneity and suggesting that the reaction of **7** with **HSA** does not modify the degree of uniformity of the size distribution of the protein system.

The ζ-potential value was not subject to variations due to the reaction of **7** with **HSA**. The surface charge of the aggregate systems retained the properties of a neutral or zwitterionic dispersion.

All these experimental results suggest that the reaction of **7** with **HSA** leads to a conformational change in **HSA** that contributes to the aggregation process of **GFA** derivatives.

Biological properties. The biological properties of **GFA** were investigated in terms of the potential ability of binding drug molecules. Thus, warfarin and diazepam were selected because these drugs are generally recognized as the gold standard molecules in such investigations. In particular, warfarin is generally recognized to bind Sudlow's site I (known also warfarin site), whereas diazepam was demonstrated to bind with high affinity to a different site (site II or diazepam site).[44] Thus, **GFA** was incubated with these drug molecules, and the fraction of the drug bound to the macromolecule was used as a measure of the binding affinity (Table 2).

Moreover, to evaluate the potential effects of the prolonged heating in the **HSA**'s ability to bind drug molecules, warfarin and diazepam were incubated in presence of native **HSA**, both before and after the treatment at 50 °C for 8 h. As reported in the Table 2, both the reaction of **HSA** with MBHA derivative **7** and the thermal treatment at 50 °C (for 8 h) of **HSA** alone appeared to produce only negligible changes in the affinity of **HSA** for the drug molecules. Thus, **GFA** appeared to retain the biological properties of native **HSA** as drug carrier and potential drug delivery system.

In vitro cytotoxicity of MBHA derivative 7

Finally, non-confluent adhered fibroblasts were incubated with increasing concentrations of MBHA derivative **7** for 24 h and then membrane integrity was evaluated by quantifying the uptake of the vital dye Neutral Red into the cells.

As shown in Figure 12, the cell toxicity of MBHA derivative **7** increased by increasing its concentration. In particular, the sample demonstrated no toxic effect toward fibroblasts for the concentration of 0.01 μg/mL as the percentage of live cells was not statistically different ($p < 0.05$) in comparison to the negative control but differed significantly from those of the positive control which had a strong cytotoxic effect. By increasing the test compound concentration at 0.1 μg/mL a reduction of cell viability of about 20% in comparison to the negative control was detected. Concerning the cytotoxicity, the standard ISO 10993–5 claims that a material can be considered as not cytotoxic if allows for a cell viability of over 70% after an exposure for 24 h. So, although the MBHA derivative **7** at 0.1 μg/mL sample affected the percentage of cell viability in comparison to the negative control, it cannot be considered cytotoxic.

At all the other concentrations ≥ 0.5 μg/mL, the test sample resulted cytotoxic but with a different extent with an IC_{50} at 1 μg/mL and a percentage of vital cells non statistically different from positive control at 5 μg/mL, i.e. the highest tested value.

Conclusions

In the aim of obtaining new fluorogenic probes potentially useful in basic amino acid labelling, the very promising optical features of previously published cinnamic derivative **6** stimulated the design of Morita-Baylis–Hillman acetate derivative **7** bearing a triphenylamine moiety. This MBHA derivative was found to show interesting AIE properties with a bright blue emission (478 nm) of its microaggregates in DMSO-water dispersions. Moreover, MBHA derivative **7** was found to react with human serum albumin (**HSA**) shifting its emission from the blue to the green-yellow (525 nm) thus leading to green fluorescent albumin (**GFA**) derivatives. Very intriguingly, **HSA** was able to transfer energy to the newly-formed cinnamic fluorophore emitting at 525 nm in **GFA** only after the thermal treatment. This result was strongly suggestive that the thermal treatment activates energy transfer by reducing the average distance between the chromophores of **HSA** and the newly-formed cinnamic fluorophore in **GFA**. In other words, the thermal treatment appeared to play a crucial role in promoting the reaction of MBHA derivative **7** that allowed the close proximity between the newly-formed cinnamic fluorophore and the tyrosine (and/or tryptophan) residues of **HSA**.

Table 2. Binding affinities of drug molecules (warfarin and diazepam) for **GFA** in comparison with native **HSA** and **HSA** after the thermal treatment at 50 °C.

	Fraction of bound drug (% ± SD)		
	GFA	HSA	HSA-50 °C
Warfarin	94.75 ± 3.87	93.59 ± 3.71	94.90 ± 4.19
Diazepam	84.09 ± 4.21	83.31 ± 3.98	83.60 ± 3.46

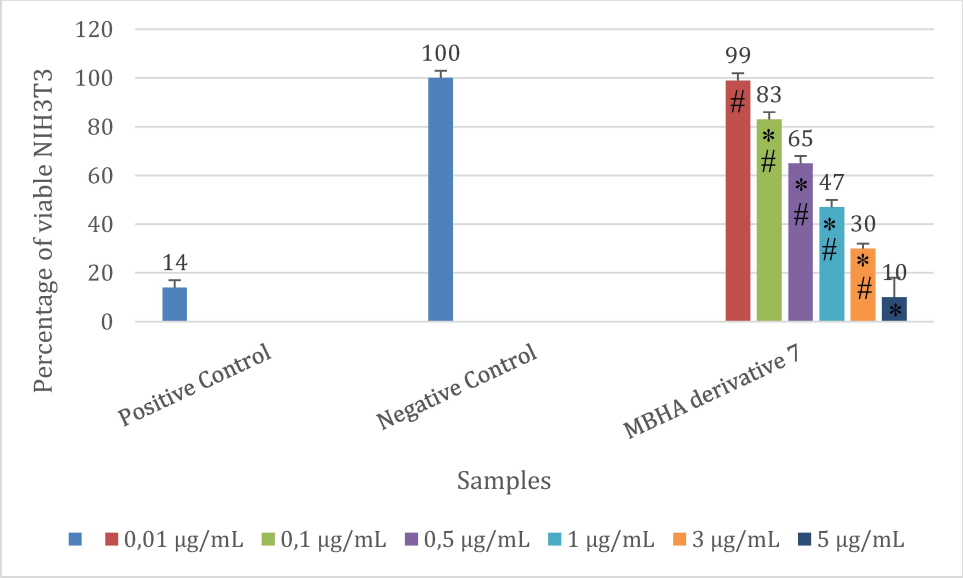

Figure 12. Percentage of viable NIH3T3 fibroblasts evaluated by the NRU assay after 24, h of contact with increasing concentrations of MBHA derivative **7**. Data are means ± SD of three experiments run in six replicates. * Value is statistically different in comparison to negative control (complete medium), $p < 0.05$. # Values are statistically different in comparison to positive control SDS, $p < 0.05$.

Docking studies suggested a possible interaction of MBHA derivative **7** with a lipophilic pocket within the **HSA** structure that could induce Lys199 to interact with the activated double bond of **7** in the addition-elimination reaction.

Characterization studies performed with **GFA** sample (i.e. SDS page experiments) demonstrated the stability of **HSA** to the reaction conditions, and DLS measurements revealed an increased propensity of **GFA** to form aggregates of well-established dimensions probably because of possible conformational changes produced by the reaction of MBHA derivative **7** with **HSA**.

The biological properties of **GFA** were investigated in terms of the potential ability of binding drug molecules such as warfarin and diazepam, which are generally recognized as standard molecules in such investigations. The results suggested that **GFA** retained the biological properties of native **HSA** as drug carrier and potential drug delivery system.

Finally, MBHA derivative **7** at 0.1 µg/mL was found to affect the cell viability in comparison to the negative control, but it cannot be considered cytotoxic at this concentration. On the other hand, at all the other tested concentrations ≥0.5 µg/mL resulted cytotoxic at a different extent with an IC_{50} at 1 µg/mL.

Experimental Section

Chemicals. Reagents, reference drugs and solvents were purchased from Sigma-Aldrich Srl (Milan. Italy). Milli-Q quality water (Millipore. Milford. MA. USA), acetonitrile (ACN) and formic acid (FA) were used for the chromatographic analyses.

Synthesis. NMR spectra were recorded with a Bruker DRX-400 AVANCE III or a Bruker DRX-600 AVANCE spectrometer in the indicated solvents: the values of the chemical shifts are expressed in ppm.

Reaction of MBHA derivative 7 with HSA. **HSA** (67 mg, 1.0 micromol) was dissolved in deuterium oxide (1.4 mL) containing phosphate buffered saline (PBS, 14 mg) at pH 7.4 into a 5 mm NMR tube and **7** (0.48 mg, 1.0 micromol) was added as a (50 mM) solution in deuterated dimethylsulfoxide (DMSO-d_6, 0.020 mL). The resulting reaction mixture was promptly analyzed by recording a ^{1}H NMR spectrum to obtain the information on the starting conditions (t = 0). The tube was then heated into an oil bath a 50 °C and ^{1}H NMR spectra were recorded at regular time intervals (i.e. 1, 2, 4, 8, 24 h).

Photophysical properties. UV-vis absorption spectra are obtained with a Perkin Elmer Lambda 900 spectrometer. PL spectra are obtained with a NanoLog composed by a iH320 spectrograph equipped with a Synapse QExtra charge-coupled device by exciting with a monochromated 450 W Xe lamp. The spectra are corrected for the instrument response.

Molecular Dynamics and Docking simulations. The crystal structure of the Human Serum Albumin, **HSA** (PDB ID 1UOR)[45] was used as a starting point for the simulations. To generate the model, we first checked the ionizable residues to determine their protonation, then the entire system was solvated with explicit water molecules and the energy minimized. To avoid excessive fluctuations of the system, initial constraints on the solute were used. The procedure using the SHAKE algorithm was employed to fix hydrogens and constrain all bonds involving hydrogen. Before the docking simulation, the protein was subjected to 20 ns of Molecular Dynamics (MD) to obtain a better sampling of the conformations. These MD simulations were executed using AMBER16 program[46] with ff14SB as the force field, at constant temperature (300°K) and pressure (1 atm) with a step size of 2 fs. Next, the lowest energy binding pose of the fully optimized compound **7** within HAS, was simulated using the DOCK6.9 algorithm.[47] The results were carefully checked, then the most representative ligand-protein complex was selected among the conformation clusters based on the lowest energy scores obtained. Further details of the procedure are reported in the Supporting Information. Thereafter, to better highlight the ligand interactions within the protein, an additional 50 ns of MD was performed.

Table 3. Chromatographic parameters adopted for the LC/UV-MS method.

Time (min)	% Eluent A H_2O (FA 0.1%v/v)	% Eluent B ACN (FA 0.1%v/v)	Flow (mL/min)	Wavelength (nm)	Scan Range (m/z)[a]
0–1	100				
15–19	20	80	0.6	254	100–2000
20	100				

[a]The detection was conducted both in positive and negative modes of ionization.

SDS page experiments. The purity of the protein samples was studied by SDS-PAGE analysis (NuPAGE 4–12% Bis-Tris protein gels; Thermo Fisher Scientific, Waltham, Massachusetts, USA).

DLS measurements. DLS measurements were performed using a Malvern Zetasizer Pro-Red (Worcestershire, UK) equipped with a 632.8 nm He–Ne laser. Samples were analyzed as synthesized without prior filtration.

Experimental measurements were performed in backscattering mode with a fixed scattering angle of 173 ° at 25 °C, after an equilibration step of 2 min. Each sample was recorded in triplicate. The correlation function was analyzed using the general purpose method to derive the intensity-weighted particle size distribution and polydispersity index.

The ζ -potential was determined at 25 °C. Electrophoretic mobility data were converted to ζ -potential (mV) using the Smoluchowski approximation. The average values of three consecutive measurements are given.

HPLC-UV/MS method. The chromatographic analyses were performed using an Agilent 1260 LC/MSD VL system (G1946 C) (Agilent Technologies. Palo Alto. CA) constituted by a vacuum solvent degassing unit, a binary high-pressure gradient pump, a 1260 series UV detector, and an 1100 MSD model VL benchtop mass spectrometer. The Agilent 6130 series mass spectra detection (MSD) single-quadrupole instrument was equipped with the orthogonal spray API-ES (Agilent Technologies. Palo Alto. CA). Nitrogen was used as nebulizing and drying gas. Chromatographic separation was performed using a Phenomenex Kinetex EVO C18–100 Å (150 mm×4.6 mm, 5 μm particle size) at room temperature (RT) and gradient elution with a binary solution was conducted as reported in Table 3.

Binging affinity to HSA, HSA-50 °C, and GFA. Warfarin and diazepam have been selected as reference compounds due to their well-known high affinity to **HSA** site I and II, respectively. The binding affinity was evaluated for both compounds by incubating in presence of a PBS 1 mM (pH 7.4) solution of **HSA** (batch n° 068 K7538 V), **HSA-50 °C**, and **GFA**. The working concentration of **HSA**, **HSA-50 °C**, and **GFA** was of 50 μM, while warfarin and diazepam were tested at the final concentration of 100 μM to ensure the affinity towards proteins and allow a suitable chromatographic response. Samples were incubated at 37 °C for 30 min, and then centrifuged at 5000 rpm for 15 minutes using centrifugal filters (Amicon Ultra®, regenerated cellulose, membrane pore size 30,000 NMWL). Filtered volumes were collected and analyzed applying the HPLC-UV/MS method described above. The percentages of bound compounds were calculated by comparison with reference solutions.

Cell Culture and in vitro Cytotoxicity Test. Cytotoxicity is defined as the degree to which a test sample induces toxicity (damage) to cells. This may occur by one or more mechanisms including damage to cell membranes. In order to evaluate the in vitro cytotoxicity of MBHA derivative **7**, the direct contact tests, proposed by ISO 10995–5 was used [ISO 10995–5:2009; Biological Evaluation of Medical Devices-Part 5: Tests for Cytotoxicity: In Vitro Methods. ISO: Geneva, Switzerland, 2009]. As the evaluation of in vitro acute toxicity does not depend on the final use for which the product is intended, the document ISO 10995–5:2009 recommends many cell lines from the American Type Collection. Among them, to test MBHA derivative **7** cytotoxicity, NIH3T3 mouse fibroblasts were chosen American Type Culture Collection (USA).

Fibroblasts NIH3T3 were propagated in DMEM supplemented with 10% fetal calf serum, 1% L-glutamine-penicillin-streptomycin solution, and 1% MEM non-essential amino acid solution, and then incubated at 37 °C in a humidified atmosphere containing 5% CO_2. Once at confluence, the cells were washed with 0.1 M PBS, separated with trypsin-EDTA solution, and centrifuged at 1000 r.p.m. for 5 min. The pellet was re-suspended in complete medium (dilution 1:15).

Cells (1.5×10^4) suspended in 1 mL of complete medium were seeded in each well of a 24 well round multidish and incubated at 37 °C in an atmosphere of 5% CO_2. After 24 h of culture, the culture medium was discharged and the MBHA derivative **7** solubilized in DMSO and diluted in complete medium, was added to each well to test increasing concentration ranging from 0.01 to 5 μg/mL. The experiment was repeated three times and each concentration was set up in six replicates. Complete medium was used as negative control and Sodium Dodecyl Sulphate (SDS) was used as positive control.

Cell toxicity, in terms of membrane integrity, of increasing concentrations of MBHA derivative **7** after 24 h of incubation towards fibroblasts NIH3T3 was evaluated by the uptake of the vital dye Neutral Red into the cells following the procedure previously reported.[48]

Acknowledgements

M.P. and A.C. acknowledge the MUR for the financial support under the project CN00000041 – "National Center for Gene Therapy and Drugsbased on RNA Technology" – CUP B63C2200061 0006 Mission 4 Component 2 (M4C2) – investment 1.4 [CN3] of the National Recovery and Resilience Plan (PNRR) funded by the European Union "Next Generation EU". M.P. acknowledge the University of Siena for the financial support of the project Chromo-GEnUP through the F-CUR2022 funding line (2265-2022-PM-CONRICMIUR_PC-FCUR2022_003). Open Access publishing facilitated by Università degli Studi di Siena, as part of the Wiley - CRUI-CARE agreement.

Conflict of Interests

The authors declare no conflict of interest.

Data Availability Statement

The data that support the findings of this study are available from the corresponding author upon reasonable request.

[1] V. K. Kadambar, A. Melman, *Adv. Exp. Med. Biol.* **2019**, *1140*, 237–250.
[2] J. Maneesh, N. Kamal, S. K. Batra, *Trends Biotechnol.* **2007**, *25*, 307–316.
[3] C. C. Ward, J. I. Kleinman, D. K. Nomura, *ACS Chem. Biol.* **2017**, *12*, 1478–1483.
[4] P. Rosa-Neto, B. Wängler, L. Iovkova, G. Boening, A. Reader, K. Jurkschat, E. Schirrmacher, *ChemBioChem* **2009**, *10*, 1321–1324.
[5] V. Raindlová, R. Pohl, M. Hocek, *Chem. Eur. J.* **2012**, *18*, 4080–4087.
[6] K. Pagano, M. Paolino, S. Fusi, V. Zanirato, C. Trapella, G. Giuliani, A. Cappelli, S. Zanzoni, H. Molinari, L. Ragona, M. Olivucci, *J. Phys. Chem. Lett.* **2019**, *10*, 2235–2243.
[7] Smith, B. D. Higgin, J. J. Raines, *Bioorg. Med. Chem. Lett.* **2011**, *21*, 5029–5032.
[8] S. B. Gunnoo, A. Madder, *ChemBioChem* **2016**, *17*, 529–553.
[9] P. G. Isenegger, B. G. Davis, *J. Am. Chem. Soc.* **2019**, *141*, 8005–8013.
[10] E. A. Hoyt, P. M. S. D. Cal, B. L. Oliveira, G. J. L. Bernardes, *Nat. Chem. Rev.* **2019**, 147–171.
[11] S. J. Walsh, S. Omarjee, W. R. J. D. Galloway, T. T.-L. Kwan, H. F. Sore, J. S. Parker, M. Hyvönen, J. S. Carroll, D. R. Spring, *Chem. Sci.* **2019**, *10*, 694–700.
[12] X. Chen, K. Muthoosamy, A. Pfisterer, B. Neumann, T. Weil, *Bioconjugate Chem.* **2012**, *23*, 500–508.
[13] M. J. Matos, B. L. Oliveira, N. Martínez-Sáez, A. Guerreiro, P. M. S. D. Cal, J. Bertoldo, M. Maneiro, E. Perkins, J. Howard, M. J. Deery, J. M. Chalker, F. Corzana, G. Jimenez-Oses, G. J. L. Bernardes, *J. Am. Chem. Soc.* **2018**, *140*, 4004–4017.
[14] E. G. Guignet, R. Hovious, H. Vogel, *Nat. Biotechnol.* **2004**, *4*, 440–444.
[15] B. A. Griffin, S. R. Adams, R. Y. Tsien, *Science* **1998**, *281*, 269–272.
[16] B. Krishnan, A. Szymanska, L. M. Gierasch, *Chem. Biol. Drug Des.* **2007**, *69*, 31–40.
[17] Z. Wang, X. Ding, S. Li, J. Shi, Y. Li, *RSC Adv.* **2014**, *4*, 7235–7245.
[18] L. Rong, C. Zhang, Q. Lei, S.-. Y. Qin, J. Feng, X.-. Z. Zhang, *Adv. Sci.* **2016**, *3*, 1500211.
[19] Z. Wang, X. Ding, S. Li, J. Shi, Y. Li, *RSC Adv.* **2014**, *4*, 7235–7245.
[20] L. D. Lavis, T. -Y Chao, R. T. Raines, *ACS Chem. Biol.* **2006**, *1*, 252–260.
[21] J. Mei, N. L. C. Leung, R. T. K. Kwok, J. W. Y. Lam, B. Z. Tang, *Chem. Rev.* **2015**, *115*, 11718–11940.
[22] D. Ding, K. Li, B. Liu, B. Z. Tang, *Acc. Chem. Res.* **2013**, *46*, 2441–2453.
[23] W. C. Wu, C. Y. Chen, Y. Tian, S. H. Jang, Y. Hong, Y. Liu, R. Hu, B. Z. Tang, Y. T. Lee, C. T. Chen, W. C. Chen, A. K. Y. Jen, *Adv. Funct. Mater.* **2010**, *20*, 1413–1423.
[24] V. Razzano, M. Paolino, A. Reale, G. Giuliani, R. Artusi, G. Caselli, M. Visintin, F. Makovec, A. Donati, F. Villafiorita-Monteleone, C. Botta, A. Cappelli, *ACS Omega* **2017**, *2*, 5453–5459.
[25] M. Saletti, J. Venditti, M. Paolino, A. Zacchei, G. Giuliani, G. Giorgi, C. Bonechi, A. Donati, A. Cappelli, *RSC Adv.* **2023**, *13*, 35773–35780.
[26] V. Razzano, M. Paolino, A. Reale, G. Giuliani, A. Donati, G. Giorgi, R. Artusi, G. Caselli, M. Visintin, F. Makovec, S. Battiato, F. Samperi, F. Villafiorita-Monteleone, C. Botta, A. Cappelli, *RSC Adv.* **2018**, *8*, 8638–8656.
[27] G. Tassone, M. Paolino, C. Pozzi, A. Reale, L. Salvini, G. Giorgi, M. Orlandini, F. Galvagni, S. Mangani, X. Yang, B. Carlotti, F. Ortica, L. Latterini, M. Olivucci, A. Cappelli, *ChemBioChem* **2022**, *23*, e202100449.
[28] M. Paolino, M. Visintin, E. Margotti, M. Visentini, L. Salvini, A. Reale, V. Razzano, G. Giuliani, G. Caselli, F. Tavanti, M. C. Menziani, A. Cappelli, *New J. Chem.* **2019**, *43*, 17946.
[29] M. Paolino, A. Reale, V. Razzano, G. Giuliani, A. Donati, C. Bonechi, G. Caselli, M. Visintin, F. Makovec, C. Scialabba, M. Licciardi, E. Paccagnini, M. Gentile, L. Salvini, F. Tavanti, M. C. Menziani, A. Cappelli, *New J. Chem.* **2019**, *43*, 6834–6837.
[30] M. Paolino, A. Reale, V. Razzano, G. Giorgi, G. Giuliani, F. Villafiorita-Monteleone, C. Botta, C. Coppola, A. Sinicropi, A. Cappelli New, *J. Chem.* **2020**, *44*, 13644–13653.
[31] M. Saletti, M. Paolino, J. Venditti, C. Bonechi, G. Giuliani, A. Boccia, C. Botta, A. Cappelli, *Dyes Pigm.* **2023**, *219*, 111571.
[32] W. J. Gradishar, D. Krasnojon, S. Cheporov, A. N. Makhson, G. M. Manikhas, A. Clawson, P. Bhar, *J. Clin. Oncol.* **2009**, *27*, 3611–3619.
[33] M. J. Hawkins, P. Soon-Shiong, N. Desai, *Adv. Drug Delivery Rev.* **2008**, *60*, 876–885.
[34] A. Spada, J. Emami, J. A. Tuszynski, A. Lavasanifar, *Mol. Pharm.* **2021**, *18*, 1862–1894.
[35] J. D. Luo, Z. L. Xie, J. W. Y. Lam, L. Cheng, H. Y. Chen, C. F. Qiu, H. S. Kwok, X. W. Zhan, Y. Q. Liu, D. B. Zhu B. Z Tang, *Chem. Commun.* **2001**, 1740–1741.
[36] E. Cariati, V. Lanzeni, E. Tordin, R. Ugo, C. Botta, A. Giacometti Schieroni, A. Sironi, D. Pasini, *Phys. Chem. Chem. Phys.* **2011**, *13*, 18005–18014.
[37] M. M. Salim, M. E. El Sharkasy, F. Belal, M. Walash, *Spectrochim. Acta Part A* **2021**, *252*, 119495.
[38] https://www.rcsb.org/structure/2BXD.
[39] G. Sudlow, D. J. Birkett, D. N. Wade, *Mol. Pharmacol.* **1975**, *11*, 824–832.
[40] U. Kragh-Hansen, *Dan. Med. Bull.* **1990**, *37*, 57–84.
[41] E. C. Meng, D. A. Gschwend, J. M. Blaney, I. D. Kuntz, *Proteins Struct. Funct. Genet.* **1993**, *17*, 266–278.
[42] E. Barratt, R. J. Bingham, D. J. Warner, C. A. Laughton, S. E. V. Phillips, S. W. Homans, *J. Am. Chem. Soc.* **2005**, *127*, 11827–11834.
[43] F. Yang, C. Bian, L. Zhu, G. Zhao, Z. Huang, M. Huang, *J. Struct. Biol.* **2007**, *157*, 348–355.
[44] G. Dargó, D. Bajusz, K. Simon, J. Müller, G. T. Balogh, *J. Med. Chem.* **2020**, *63*, 1763–1774.
[45] X. M. He, D. C. Carter, *Nature* **1993**, *364*, 362.
[46] D. A. Case, R. M. Betz, D. S. Cerutti, T. E. Cheatham, III, T. A. Darden, R. E. Duke, T. J. Giese, H. Gohlke, A. W. Goetz, N. Homeyer, S. Izadi, P. Janowski, J. Kaus, A. Kovalenko, T. S. Lee, S. LeGrand, P. Li, C. Lin, T. Luchko, R. Luo, B. Madej, D. Mermelstein, K. M. Merz, G. Monard, H. Nguyen, H. T. Nguyen, I. Omelyan, A. Onufriev, D. R. Roe, A. Roitberg, C. Sagui, C. L. Simmerling, W. M. Botello-Smith, J. Swails, R. C. Walker, J. Wang, R. M. Wolf, X. Wu, L. Xiao and P. A. Kollman (**2016**), AMBER 2016, University of California, San Francisco.
[47] https://onlinelibrary.wiley.com/doi/epdf/10.1002/jcc.23905.
[48] S. Lamponi, M. C. Baratto, E. Miraldi, G. Baini, M. Biagi, *Plants* **2021**, *10*, 97.

Manuscript received: February 24, 2024
Revised manuscript received: January 24, 2024
Accepted manuscript online: February 18, 2024
Version of record online: March 13, 2024